Published in final edited form as:
J Med Chem. 2013 August 22; 56(16): 6521–6530. doi:10.1021/jm400914r.

A dynamic G-quadruplex region regulates the HIV-1 long terminal repeat promoter

Rosalba Perrone[a], **Matteo Nadai**[a], **Ilaria Frasson**[a], **Jerrod A. Poe**[b], **Elena Butovskaya**[a], **Thomas E. Smithgall**[b], **Manlio Palumbo**[c], **Giorgio Palù**[a], and **Sara N. Richter**[a,*]

[a]Department of Molecular Medicine, via Gabelli 63, 35121 Padua, Italy

[b]Department of Microbiology and Molecular Genetics, University of Pittsburgh School of Medicine, Pittsburgh, PA, USA

[c]Department of Pharmaceutical and Pharmacological Sciences, via Marzolo 5, 35131 Padua, Italy

Abstract

G-quadruplexes, non-canonical nucleic acid structures, act as silencers in the promoter regions of human genes; putative G-quadruplex forming sequences are also present in promoters of other mammals, yeasts and prokaryotes. Here we show that also the HIV-1 LTR promoter exploits G-quadruplex-mediated transcriptional regulation with striking similarities to eukaryotic promoters and that treatment with a G-quadruplex ligand inhibits HIV-1 infectivity. Computational analysis on 953 HIV-1 strains substantiated a highly conserved G-rich sequence corresponding to Sp1 and NF- □B binding sites. Biophysical/biochemical analysis proved that two mutually exclusive parallel-like intramolecular G-quadruplexes, stabilized by small molecule ligands, primarily fold in this region. Mutations disrupting G-quadruplex formation enhanced HIV promoter activity in cells, whereas treatment with a G-quadruplex ligand impaired promoter activity and displayed antiviral effects. These findings disclose the possibility of inhibiting the HIV-1 LTR promoter by G-quadruplex-interacting small molecules, providing a new pathway to development of anti-HIV-1 drugs with unprecedented mechanism of action.

Introduction

G-rich sequences in DNA may associate to form four-guanine square planar structures called G-quartets which give rise to G-quadruplexes by stacking on top of each other. G-quadruplexes are polymorphic intra- or inter-molecular four-stranded structures, and the adopted structures depend on base sequence, strand concentration, loop connectivities, and cations present. DNA strands in G-quadruplex take anti-parallel, parallel, or hybrid conformations, and the nucleotide linkers between G-quartets can adopt a multitude of loop structures[1].

G-quadruplexes are involved in several key biological functions[2]. In particular, tight clusters of putative G-quadruplex-forming sequences are located immediately upstream and downstream of the transcription start site in proliferation-associated genes[3, 4]. Notably, G-quadruplexes are found in the promoters of a wide range of genes important in cell signaling, having representatives from the six hallmarks of cancer[5]. Strong evidence of G-

Corresponding Author: Sara N. Richter, ph: +39 049 8272346; sara.richter@unopd.it.

Supporting Information Available: Supporting Figures S1–S8 and Tables S1–S2. This material is available free of charge via the Internet at http://pubs.acs.org.

quadruplex formation inside human cells has been recently provided by an antibody-based approach[2]; moreover, G-quadruplex stabilizing and destabilizing proteins have been identified[6, 7].

The biological relevance of G-quadruplex structures prompted the development of a diverse array of G-quadruplex ligands. Their general features comprise a large flat aromatic surface and cationic groups[8]: examples include perylenes (PIPER), porphyrins, (TMPyP4), and trisubstituted acridines (BRACO-19).

Besides humans, other mammals[9], yeasts[10] and prokaryotic cells[11–13] also exhibit putative G-quadruplex forming sequences in regions proximal to the transcription start sites of protein-coding genes. Other organisms, such as viruses, might have evolved analogous regulatory mechanisms, but research in this area has not been explored.

Few data are available on the presence of G-quadruplexes in HIV-1: it has been demonstrated that a single-stranded portion (central DNA flap) of the reverse-transcribed pre-integration HIV-1 genome forms a G-quadruplex structure that specifically interacts with the viral nucleocapsid protein thereby protecting the pre-integrated genome from nuclease degradation[14]. Furthermore, a G-quadruplex structure apparently promotes dimerization of the two viral RNA genome copies[15]. In the proviral genome, however, no G-quadruplex structures have been reported.

Within the integrated provirus, the HIV-1 long terminal repeat (LTR) governs transcription of viral genes and the full-length genome[16, 17]. Two identical LTR sequences are located at both extremes of the HIV-1 provirus, each composed of three regions: U3, R and U5. The U3 promoter region can be divided in three functional sections: an upstream regulatory element (−454 to −104) including binding sites for cellular transcription factors, an enhancer (−105 to −79) with two binding sites for the nuclear factor κB (NF-κB), and the core promoter (−78 to −1) composed of three tandem binding sites for specificity protein 1 (Sp1) and a TATA box. The R (+1 to +96) region contains the unique transactivation response enhancer TAR (+1 to +60), which modulates Tat activation[18].

Transcription of the HIV-1 provirus starts when the U3 promoter sequence binds cellular factors, including NF-κB, Sp1, the TATA box binding protein, and RNA polymerase II[16]. The transcription complex allows low-level production of viral transcripts. Interaction of the viral protein Tat with the 5'-end of nascent viral transcripts greatly amplifies gene expression[19].

Genetic variability within LTR binding sites in U3 and TAR regions has been observed in several HIV-1 subtypes[20, 21]. However, NF-κB and Sp1 binding sites are remarkably conserved[22].

Here we show the first evidence of dynamic regulatory G-quadruplexes in the HIV-1 LTR region. Specifically, the conserved region encompassing NF-κB site and Sp1 sites contains G-tracts involved in two mutually exclusive G-quadruplex structures. G-quadruplex ligands greatly stabilized these conformations and induced folding and stabilization of an additional quadruplex. Mutations abolishing G-quadruplex formation enhanced LTR promoter activity, while G-quadruplex ligands depleted promoter activity and exerted antiviral activity, indicating a regulatory role for LTR G-quadruplexes and their possible exploitation as therapeutic targets.

Results

Putative G-quadruplex sequences are present in the NF-κB and Sp1 binding sites of the HIV-1 LTR promoter region

The U3 region of the HIV-1 LTR (representative strain HXB2_LAI; NC_001802) is very rich in G bases: the segment corresponding to part of the core promoter and enhancer (positions −105/−48 with respect to the transcription initiation site) consists of 50% G and 70% GC. Gs were mainly clustered in groups of 2–4 continuous G bases (Fig. 1A). Because of these features, the possibility of G-quadruplex folding was analyzed using an online algorithm-based software for recognition of putative Quadruplex forming G-Rich Sequences (QGRS Mapper)[23]. Putative QGRS were ranked based on G-score, the likelihood to form a stable G-quadruplex. Twelve putative sequences were found (Table S1): 3 sequences, namely LTR-I, -II and -III, were composed of GGG repeats (numbered 1–6, Fig. 1A) and could thus generate G-quadruplexes with 3 stacked G-quartets exhibiting the highest G-scores. These sequences differed by the length of the loop segments connecting G-tracts (Table S1). The remaining 9 sequences involved 2 stacked quartets and were ranked with lower G scores (Fig. S1A).

Interestingly, the G-rich −105/−48 tract was also the binding region of two important cellular transcription factors that stimulate viral transcription: NF- □B, with two binding sites at −105/−96 and −92/−82, and Sp1, three molecules of which bind at −79/−68, −67/−57 and −56/−48[17] (Fig. 1A). To establish the importance of these predicted sequences within a viral context, the degree of base conservation among HIV-1 strains was assessed. Among 953 analyzed LTR sequences, most Gs and also non-G bases were highly conserved (Fig. S1B).

Two stable G-quadruplexes form in the HIV-1 LTR

The three LTR sequences, namely LTR-I, -II and –III, embedding four GGG tracts each (Fig. 1A) and displaying higher G-scores (Table S1), were selected and analyzed for their ability to form G-quadruplexes. Circular dichroism (CD) spectroscopy was initially performed in the absence or presence of increasing concentrations of K^+ to monitor G-quadruplex formation and its likely topology. LTR-II and LTR-III produced CD spectra characteristic of a G-quadruplex structure in a K^+-dependent manner (Fig. 1B, Fig. S2A). Spectra of both oligonucleotides exhibited a positive band at 266 nm and a negative peak at 244 nm, a signature suggesting a parallel-like G-quadruplex[24, 25]. In contrast, LTR-I showed a negative band at 240 nm, a shoulder at 260 nm and a positive peak at 280 nm, and low K^+-dependence, features not typical of G-quadruplex structures (Fig. S2A). The topology of the selected sequences was further assessed by UV thermal difference spectroscopy (TDS). LTR-II and LTR-III produced TDS signatures with three positive bands at 275, 257 and 239 nm, and three negative bands at 296, 261 and 252 nm, characteristic of the G-quadruplex structure[26] (Fig. 1C). In addition, the TSD factor, calculated as $\square A_{240nm}/\square A_{295nm}$ was above 5, indicating a parallel-like topology (Fig. 1C; inset)[24]. In contrast, the TDS signature of LTR-I was not representative of G-quadruplex (Fig. S2B).

Further support for the formation of G-quadruplexes was obtained by protection assays. Two G-N7 alkylators were separately employed: DMS, the standard reactant to highlight G bases involved in G-quartets, and clerocidin (CL), endowed with finely tunable reactivity[27, 28]. In the CL protection assay, tracts 2, 3, 4 and 5 in the LTR-II sequence were all protected (Fig. 1D). In particular, in G-tract 2, the three 5'-Gs were involved in G-quadruplex, while the 3'-G was excluded (symbol *, lane 10). Surprisingly, in tract 3 the 5'-G was overexposed to cleavage (symbol ¤, lane 10). Based on CL discrimination between protected and stretched bases[28], the cleaved G, adjacent to the 8-nt-long linker region, is likely strained and therefore exposed to CL alkylation. In the LTR-III sequence, tracts 3, 4, 5, and 6 were

clearly protected, while the 3'-G of tract 6 was not (symbol *, lane 15). Conversely, no protection was observed in the LTR-I sequence (lanes 1–5). Similar results were obtained using the G-N7 alkylator DMS (Fig. S3).

Stability of LTR-II and LTR-III G-quadruplexes in the absence/presence of 100 mM K^+ was next assessed by melting experiments monitored by CD (Table 1 and Fig. S4A). In the presence of K^+, LTR-III was 4°C more stable than LTR-II; T_m values of LTR-II and LTR-III unfolding were 2.6°C and 1.8°C (respectively) higher than T_m values gained during the refolding process (Fig. S4B). The small hysteresis was indicative of reversible and intramolecular G-quadruplex formation, with folding kinetics faster for LTR-III than for LTR-II. These data indicate that the presence of two long loops in LTR-II (9, 11, 1 nt-loops) versus only one long loop in LTR-III (11, 1, 3 nt-loops) moderately affected both the thermodynamic stability and the kinetics of G-quadruplex formation. UV melting experiments at 4 μM and 60 μM oligomer concentrations resulted in superimposable T_m values, confirming intramolecular G-quadruplex formation (Fig. S4C).

The commercially available G-quadruplex ligands TMPyP4, BRACO-19 and PIPER were next tested by CD for binding to the novel LTR G-quadruplex structures in the absence/presence of 100 mM K^+. In the presence of K^+, the average ΔT_m was above 30°C indicating both LTR sequences were significantly stabilized by the compounds. BRACO-19 was most efficient, followed by TMPyP4; PIPER was less effective, especially with LTR-III. Interestingly, even in the absence of K^+, compounds induced a G-quadruplex conformation with average ΔT_m around 15°C (Table 1). Further evidence of the stability of the LTR G–quadruplexes was provided by Taq polymerase stop assay (Fig. 1E). Samples were incubated in the absence/presence of 100 mM K^+ (lanes 1 and 2), and with increasing concentrations (50–100 nM) of TMPyP4 (lanes 3 and 4). TMPyP2, a non-G-quadruplex binding porphyrin[29], was used as a negative control (lanes 5–6). Taq polymerase activity was tested at 47°C against LTR-I, LTR-II and LTR-III DNA templates. Full-length products were obtained in the absence of K^+ in the three sequences. However, in the presence of K^+, a premature stop site occurred in LTR-II and LTR-III (lanes 2) at the first two 3'-G bases involved in G-quadruplex (G-tract 5 in LTR-II and 6 in LTR-III). The stop became clearer upon incubation with TMPyP4 (lanes 3–4). The stop observed in the presence of TMPyP2 was comparable to the stop with K^+ alone (compare lanes 5–6 with 2), confirming that the compound did not affect G-quadruplex formation. In addition, no stop was observed in LTR-I, showing that polymerase activity was not directly inhibited by the compounds (LTR-I, lanes 2–6).

Multiple G-quadruplexes form in the full-length LTR G-rich region

The full-length LTR G-rich sequence comprises 4 GGG-tracts (1, 3–5), 2 GGGG-tracts (2, 6) and 3 additional GG-tracts (3', 3", 6') which could be used for multiple G-quadruplex formation (Fig. 1A and Fig. S1A).

We examined a number of sub-sequences to dissect this issue, corresponding to LTR-II, LTR-III and their combination of LTR-(II+III).

Melting experiments—CD-monitored melting experiments (Table 1) showed that the melting temperatures of LTR-II and LTR-III increased by 10–13°C in the presence of K^+. LTR-(II+III) and the full length LTR (FL-LTR) were also greatly stabilized by the metal ion, T_ms being very close to each other and 4–6°C higher than for LTR-II and LTR-III. G-quadruplex ligands further stabilized these conformations (Table 1).

Footprinting studies—LTR-(II+III) and FL-LTR were next examined in a CL-protection assay (Fig. 2). In the LTR-(II+III) sequence, all G-tracts present (2–6) were protected

indicating the coexistence of LTR-II and LTR-III structures (compare lanes 5 and 4, Fig. 2A). In the FL-LTR, G-tract 1 was not protected (compare lanes 4 and 3, Fig. 2B), showing its exclusion from G-quadruplex folding. In the 3'-region of FL-LTR, magnified in Fig. 2C, G-tracts 4, 5 and 6 were clearly protected (compare lanes 4 and 3, Fig. 2C). Tracts 3 and 2 were partially protected (G −77, G −90 and G −87) and partially overexposed (G −76, G −78 and G −89) (symbols * and ¤, respectively, lane 4, Fig. 2C), indicating involvement of these tracts in the G-quadruplex, with buried and stretched bases. In addition, G-71 was protected suggesting participation in the G-quadruplex conformation or burial within the long linker region possibly folded on the quadruplex core. These data imply that both LTR-II and LTR-III conformations form in the FL-LTR. To note that similar dynamic G-quadruplexes have been previously proposed[30]. In addition, both LTR-II and LTR-III display a 11-bp long loop that could form 4 Watson-Crick base pairs and a GTG hairpin. Similar folding in the loop of the hTERT promoter G-quadruplex structure has been shown to promote cooperative binding[31, 32]. However, based on the footprinting data, such a folding does not likely occur in the LTR G-quadruplexes.

Taq polymerase stop assays—In Taq polymerase stop assays, at increasing concentrations of K^+, pausing sites were observed at all G-quadruplex relevant G-tracts, i.e. 6, 5, 4, 3 and 2 (lanes 2–4, Fig. 3A), confirming the coexistence of LTR-II and LTR-III structures. With TMPyP4, two major stops emerged at G-tracts 6 and 5, while pausing at G-tracts 4–2 was no longer observed (lanes 5–6). Using BRACO-19, an identical behavior was obtained (lanes 9–10), whereas the control compound TMPyP2 maintained a stop site pattern similar to that observed in K^+ alone (lanes 7–8). The strong stabilization imparted by the ligands (see Table 1) apparently caused the polymerase to stop at the first G repeat involved in a G-quadruplex, without allowing the enzyme to further proceed on the DNA template. We concluded that BRACO-19 and TMPyP4 mainly stimulated formation of an LTR-III-like structure and in part of an LTR-II-like structure (3'-stops at 6 and 5, respectively, Fig. 3A).

A novel drug-induced LTR structure—Interestingly, a new pausing site arose at G-tract 6', which suggests the formation a new LTR structure (LTR-IV).

Single-base mutations were next introduced in the FL-LTR to assess the role of each G-tract on G-quadruplex formation. Mutants were evaluated in the absence/presence of BRACO-19 and TMPyP4. In the presence of BRACO-19, deletion of one G base in G-tract 6 (m6) resulted in maintenance of the third stop site only at G-tracts 5/4 (formation of only LTR-II, Fig. 3B). Mutations in G-tracts 5 and 4 (m5 and m4) produced the harshest effects with all stops removed (no LTR G-quadruplex formed). Mutation in G-tract 3 (m3) increased the efficiency of the newly proposed first stop site (LTR-IV), while removal of one G in G-tract 6' (m6') effectively deleted the first stop (only LTR-II and LTR-III formed). Mutation in G-tract 2 (m2) hampered formation of the third stop (no LTR-II), while mutations in G-tracts 1 (m1), 3' (m3') and 3" (m3") produced no effect. Similar results were obtained with TMPyP4 (Fig. S5).

Deletion of G-tracts m6', m6, m5 and m4 inhibited formation of LTR-IV, indicating that these G-tracts must all be involved in its structure. The 19-bp LTR-IV sequence including these G-tracts revealed CD and UV features characteristic of a parallel G-quadruplex (Fig. S6), showing increased stability upon K^+ addition (Table 1). Although in the presence of 100 mM K^+ LTR-IV was less stable than LTR-II, LTR-III, LTR-(II+III) and LTR-FL, upon addition of G-quadruplex ligands, LTR-IV stability significantly increased (Table 1); in particular, T_m values of LTR-IV in the presence of ligands were consistently higher than T_m of LTR-III and LTR-II (Table 1). These data corroborate the results presented in Fig. 3A and 3B and demonstrate that G-quadruplex ligands both stabilize naturally-occurring G-

quadruplex conformations and induce (and greatly stabilize) a novel G-quadruplex structure which is not present under physiological conditions. Interestingly, LTR-IV could form a G-quadruplex with a single bulge, a type of structure recently reported in G-quadruplex conformations[33].

Based on these data, involvement of G-tracts and G-quadruplex types could be extrapolated as shown in Fig. 3C and Fig. S7. In the WT sequence, in the presence of ligands, three G-quadruplexes corresponding to LTR-II, LTR-III and LTR-IV are present. The core of the LTR G-quadruplex architecture rests on G-tracts 4 and 5 whose mutations completely abolish quadruplex building.

G-quadruplex structures regulate HIV-1 LTR promoter activity

To evaluate the biological significance of G-quadruplex structures within the LTR sequence, the WT LTR sequence (nts −381/+83) and selected point mutants were cloned upstream of the firefly luciferase gene in a promotorless plasmid. A control vector with *Renilla* luciferase under the HSV-1 TK promoter was used to normalize transfection efficiency. Mutants corresponding to m4 and m5, which totally prevent G-quadruplex formation as described above, were assayed along with WT FL-LTR and mutant m3" which served as controls, respectively, for the original G-quadruplex-forming sequence and for a mutated sequence that does not disrupt G-quadruplex. LTR promoter activity was tested in HEK 293T cells: m4 and m5 LTR promoter activities were about twice as high as that of the WT LTR (Fig. 4A). This increment is in line with that observed in eukaryotic promoters, i.e. human c-Myc, KRAS and *thymidine kinase 1*[34–36]. In contrast, when G-quadruplex formation was unharmed (m3"), LTR promoter activity was comparable to wild-type. These data suggest that G-quadruplexes act as repressor elements in the transcriptional activation of HIV-1.

The promoter activities of WT and m5 LTRs were next tested in the presence of increasing concentrations of BRACO-19. As shown in Fig. 4B, WT LTR promoter activity decreased to ~70% of the untreated control, while displaying no effect on m5 LTR activity, supporting a G-quadruplex-mediated inhibition. We also observed concentration-dependent inhibition of the control *Renilla* luciferase reporter gene by BRACO-19 (less intense than inhibition of the LTR-driven firefly luciferase) attributable to the toxic effects produced by ligand binding to eukaryotic G-quadruplex structures (data not shown). A similar effect has been previously observed[34]. Therefore, the effects of G-quadruplex ligands were next evaluated in a GFP-reporter system in the presence/absence of the transcriptional activator Tat, using flow cytometry to gate only GFP+ cells with viable morphology. In the presence of Tat, BRACO-19 was able to impair LTR promoter activity in a dose-dependent fashion (~50% inhibition at 6 μM, Fig. 4C). Moreover, in the absence of Tat, inhibition was 30%, confirming the results obtained in the luciferase assay. In contrast, the control ligand TMPyP2 did not show significant inhibition under these conditions (Fig. S8). Because Tat-mediated trans-activation boosts viral transcription acting on early mRNA transcripts originating by LTR-mediated transcription, when the latter is blocked, a magnified inhibition may be observed in the presence of Tat.

The G-quadruplex ligand, BRACO-19, displays antiviral activity

Having observed a reduction in HIV LTR-driven promoter activity, we next assayed the most active compound, BRACO-19, for antiviral activity. For these experiments, we used the TZM-bl assay, in which HIV infection drives transcription of an HIV-1 LTR-luciferase reporter gene construct[37]. We observed a significant inhibition of HIV-dependent gene expression upon treatment with the G-quadruplex ligand (Fig. 4D) at ligand concentrations that did not affect cell viability (Fig. S8C). HIV LTR activity in TZM-bl cells has been

previously reported to be sensitive to the HIV accessory protein Nef[38]. To rule out a role for Nef in BRACO-19-mediated inhibition, the same experiment was repeated with Nef-defective HIV (MNef). A similar inhibitory effect was observed indicating that the effect of BRACO-19 is Nef-independent. In contrast, the control ligand TMPyP2 did not affect LTR activity in response to either virus (Fig. S8B). These data indicate that G-quadruplex ligands significantly inhibit HIV-1 and that this effect may depend on stabilization of G-quadruplex structures within the HIV-1 LTR promoter region.

Discussion

We have presented the first evidence of a regulatory G-quadruplex-forming region in the HIV-1 LTR promoter. All main G-quadruplexes identified, i.e. LTR-III, LTR-II and LTR-IV, displayed sequence and structural features typical of G-quadruplexes previously implicated in regulation of the promoter activity of eukaryotic oncogenes, i.e. parallel-like topology, $G_3N_1G_3$ motif (i.e. G_3CG_3)[39], and silencing effect on promoter activity[35, 36, 40–42].

Notably, a lentiviral plasmid engineered with point mutations in the Sp1 binding sites, mimicking our LTR-III-disrupting mutants (i.e. m4 or m6), reported reduced occupancy by HDAC1 resulting in 2–3 fold increased rates of spontaneous transcription activation compared to the WT-provirus[17]. It is therefore conceivable that HDAC1 participates in stabilization of LTR G-quadruplexes to down-regulate viral transcription.

The above described features point out the biological relevance of the G-quadruplex forming region in the HIV-1 promoter. This novel notion opens up the possibility of inhibiting the HIV-1 LTR promoter activity by G-quadruplex interacting small molecules. Presently, a major disadvantage of existing G-quadruplex ligands is that they recognize the quadruplex core without being able to finely discriminate between G-quadruplex structures. Here we have nonetheless shown that BRACO-19 is effective towards the virus with minimal effect on cell viability. Therefore a therapeutic window can be envisaged that would consent the employment of known G-4 binders as anti-HIV compounds. In addition, based on the sequence and structural differences between the LTR and eukaryotic G-quadruplexes, rational design of small-molecules may be envisaged for the development of anti-HIV-1 drugs with an unprecedented mechanism of action.

Experimental Section

Materials

Oligonucleotides were from Sigma-Aldrich (Milan, Italy) (Table S1). Clerocidin (CL) was a gift of Leo Pharmaceutical Products (Ballerup, Denmark). Dimethylsulfate (DMS) was from Sigma Aldrich, TMPyP4 and PIPER from Calbiochem, (Merck Chemicals, Nottingham, UK), BRACO-19 from ENDOTHERM, (Saarbruecken, Germany). T4 polynucleotide kinase was from Invitrogen (Paisley, UK), [□^{32}P]ATP from Perkin Elmer (MA, USA).

G-quadruplex analysis of the HIV-1 LTR region

The HIV-1 LTR region (strain HXB2_LAI; NC_001802) was analyzed by QGRS Mapper (http://bioinformatics.ramapo.edu/QGRS/index.php) for prediction of G-4 forming sequences in both coding and non-coding strands. The following restrictions were applied: maximum length 30 nt; minimum G-group size 2 nt; loop size 0–15 nt. Conserved bases were evaluated by aligning LTR U3 sequences from the HIV database (http://www.hiv.lanl.gov/content/sequence/NEWALIGN/align.html) using Jalview (http://www.jalview.org/).

Spectroscopic analysis

For CD analysis, all DNA oligonucleotides were diluted from stock to final concentration (4 μM) in lithium cacodylate buffer (10 mM, pH 7.4) and, where appropriate, KCl. All samples were annealed by heating at 95 °C for 5 min, gradually cooled to room temperature and measured after 24 h. Compounds at 16 μM final concentration were added after DNA annealing. CD spectra were recorded on a Jasco-810 spectropolarimeter (Jasco, Easton, MD, USA) equipped with a Peltier temperature controller using a quartz cell of 5-mm optical path length and an instrument scanning speed of 100 nm/min with a response time of 4s over a wavelength range of 230–320 nm. The reported spectrum of each sample represents the average of 2 scans at 20°C and is baseline-corrected for signal contributions due to the buffer. Observed ellipticities were converted to mean residue ellipticity (θ) = deg × cm^2 × $dmol^{-1}$ (mol. ellip.). For the determination of T_m, spectra were recorded over a temperature range of 20–95 °C, with temperature increase of 5 °C/min or 2°C/min, followed by an equilibration step of 1 min. As previously described, T_m values were calculated according to the van't Hoff equation, applied for a two state transition from a folded to unfolded state, assuming that the heat capacity of the folded and unfolded states are equal[43, 44]. For thermal difference spectrum (TDS) analysis, UV spectra were recorded on Lamba25 UV/Vis spectrometer (Perkin Elmer) equipped with a Peltier temperature controller. TDS spectra were calculated by subtracting the spectrum at each temperature from the spectrum at 95°C. TDS factors were calculated as the absolute values of $\Delta A_{240nm}/\Delta A_{295nm}$, where ΔA_λ is the difference, at the given wavelength λ between the absorbance above and below the melting.

Taq polymerase stop assay

Primer (LTR G4 Taq primer, Table S1) was 5'-end labelled with [γ_{32}P]ATP using T4 polynucleotide kinase at 37°C for 30 min. The labelled primer (72 nM), annealed to the template (36 nM) in lithium cacodylate buffer (10 mM, pH 7.4), was extended with Ampli*Taq* Gold DNA polymerase (2U/reaction, Applied Biosystem, California) at 47°C for 30 min. Where specified, samples were incubated with G-quadruplex-ligands and 100 mM KCl for 20 min at room temperature and primer extension performed as described. Reactions were stopped by EtOH precipitation, extension products were separated on 12% denaturing gel, visualized by phosphorimaging (Typhoon FLA9000, GE Healthcare).

Footprinting assays

Clerocidin and DMS-mediated footprinting assays were performed as previously described[28].

Plasmid construction

The LTR DNA region was amplified by PCR on the HIV-1 genome (AF033819.3) using reported primers (Table S1). The LTR amplicon was subcloned into pGL4.10-Luc2 (Promega) within XhoI and HindIII sites. The resulting pGL4.10-Luc2/LTR vector contained the sequenced 464 bp-long LTR-region (corresponding to nts −381/+83 in the HIV-1 genome) fused to the luciferase coding region. Mutant pGL4.10-Luc2/LTR vectors were generated using QuikChange mutagenesis kit (Stratagene/Agilent Technologies) and primers (Table S1).

Reporter assays

Vectors pGL4.10Luc2/LTR and pGL4.74 (200 ng each) were transfected in 5.5×10^4 HEK 293T cells per well onto 96-well plates, using *Trans*IT-293 Transfection Reagent (Mirus Bio LLC). Plasmid pGL4.74-hRLUC/TK (Promega), containing a *Renilla* luciferase gene driven by the *Herpes Simplex* virus thymidine kinase promoter, was used as a control for transfection efficiency. Expression of firefly luciferase, with respect to that of *Renilla*

luciferase, was determined 24 h after transfection using Dual-Glo Luciferase Assay System (Promega). Cell lysate (75 μL) was mixed with reconstituted Dual-Glo Luciferase Buffer (75 μL) or Dual-Glo Stop&Glo Buffer, and light output detected with VICTOR X2 Multilabel Plate Reader (Perkin Elmer). Luciferase and *Renilla* output ratio was calculated.

For the LTR-GFP reporter assay, 2×10^5 of HEK 293T cells in 6-well plates were transfected with pcLTR-EGFP DNA 3.1. After 4 h, cells were treated with BRACO-19 or TMPyP2 and incubated over-night. To evaluate mean of EGFP fluorescence, a total of 30000 events were acquired for each sample with an LRS 2 instrument using FACS DIVA Software (BD Bioscience) and analyzed with Flow Jo (Tree Star).

Antiviral assays

Viral stocks were prepared by transfection of HEK 293T cells with wild-type and Nef-defective (Nef) proviral genomes (NL4-3 strain) and amplified in the T cell line, MT2 (NIH AIDS Research and Reference Reagent Program) as previously described[45, 46]. Viral transcription was measured using the TZM-bl reporter cell line which contains a luciferase reporter under the control of the HIV-1 LTR[37] (NIH AIDS Research and Reference Reagent Program). Cells were seeded in 96-well plates (2×10^4) and grown overnight. BRACO-19 and TMPypP2 were preincubated separately with both cell culture medium (100 μL) and wild-type HIV-1 or Nef HIV-1 (100 μL) for 4 h prior to infection in a combined final volume of 200 μL. After 48 h at 37°C, cells were washed with PBS and lysed in luciferase lysis buffer (Promega). Lysates (40 μL) with 50 μL luciferase reagent (Promega) were read with a delay time of 2 s and an integration period of 10 s.

Cytotoxicity Assays

TZM-bl cells[37] were seeded in 96-well plates (2×10^4), grown overnight incubated with compounds in DMSO carrier solvent and incubated at 37°C. After 48 h, cytotoxicity was assessed using the Cell Titer Blue reagent (Promega).

Supplementary Material

Refer to Web version on PubMed Central for supplementary material.

Acknowledgments

We thank Dr. I. Mičetić (European Center for the Sustainable Impact of Nanotechnology, Rovigo, Italy) for assistance in G-4 analysis of HIV-1 strains. Profs. C. Parolin, A. Loregian and Dr. B. Mantelli (Dept. Molecular Medicine, University of Padua, Italy) are kindly acknowledged for providing the wild-type LTR sequence (GenBank AF033819.3), pcLTR-EGFP DNA, and providing assistance with the FACS instrument, respectively. This work was supported by the Bill&Melinda Gates Foundation through the Grand Challenges Explorations Initiative (GCE grant #OPP1035881 to SNR), by the Italian Ministry of University and Research (FIRB-Ideas RBID082ATK_001 to SNR), by the University of Padua and by National Institutes of Health Grant AI57083 (to TES).

Abbreviations

G	guanine
LTR	long terminal repeat
TDS	thermal difference spectrum
DMS	dimethyl sulfate
CL	clerocidin

Tm Temperature of melting

References

1. Huppert JL. Structure, location and interactions of G-quadruplexes. Febs J. 2010; 277:3452–3458. [PubMed: 20670279]
2. Biffi G, Tannahill D, McCafferty J, Balasubramanian S. Quantitative visualization of DNA G-quadruplex structures in human cells. Nat Chem. 2013; 5:182–186. [PubMed: 23422559]
3. Huppert JL, Balasubramanian S. G-quadruplexes in promoters throughout the human genome. Nucleic Acids Res. 2007; 35:406–413. [PubMed: 17169996]
4. Eddy J, Maizels N. Conserved elements with potential to form polymorphic G-quadruplex structures in the first intron of human genes. Nucleic Acids Res. 2008; 36:1321–1333. [PubMed: 18187510]
5. Balasubramanian S, Hurley LH, Neidle S. Targeting G-quadruplexes in gene promoters: a novel anticancer strategy? Nat Rev Drug Discov. 2010; 10:261–275. [PubMed: 21455236]
6. Gonzalez V, Hurley LH. The c-MYC NHE III(1): function and regulation. Annu Rev Pharmacol Toxicol. 2010; 50:111–129. [PubMed: 19922264]
7. Cogoi S, Paramasivam M, Spolaore B, Xodo LE. Structural polymorphism within a regulatory element of the human KRAS promoter: formation of G4-DNA recognized by nuclear proteins. Nucleic Acids Res. 2008; 36:3765–3780. [PubMed: 18490377]
8. Ou TM, Lu YJ, Tan JH, Huang ZS, Wong KY, Gu LQ. G-quadruplexes: targets in anticancer drug design. Chem Med Chem. 2008; 3:690–713. [PubMed: 18236491]
9. Verma A, Halder K, Halder R, Yadav VK, Rawal P, Thakur RK, Mohd F, Sharma A, Chowdhury S. Genome-wide computational and expression analyses reveal G-quadruplex DNA motifs as conserved cis-regulatory elements in human and related species. J Med Chem. 2008; 51:5641–5649. [PubMed: 18767830]
10. Hershman SG, Chen Q, Lee JY, Kozak ML, Yue P, Wang LS, Johnson FB. Genomic distribution and functional analyses of potential G-quadruplex-forming sequences in Saccharomyces cerevisiae. Nucleic Acids Res. 2008; 36:144–156. [PubMed: 17999996]
11. Beaume N, Pathak R, Yadav VK, Kota S, Misra HS, Gautam HK, Chowdhury S. Genome-wide study predicts promoter-G4 DNA motifs regulate selective functions in bacteria: radioresistance of D. radiodurans involves G4 DNA-mediated regulation. Nucleic Acids Res. 2013; 41:76–89. [PubMed: 23161683]
12. Rawal P, Kummarasetti VB, Ravindran J, Kumar N, Halder K, Sharma R, Mukerji M, Das SK, Chowdhury S. Genome-wide prediction of G4 DNA as regulatory motifs: role in Escherichia coli global regulation. Genome Res. 2006; 16:644–655. [PubMed: 16651665]
13. Wieland M, Hartig JS. Investigation of mRNA quadruplex formation in Escherichia coli. Nat Protoc. 2009; 4:1632–1640. [PubMed: 19876023]
14. Lyonnais S, Gorelick RJ, Mergny JL, Le Cam E, Mirambeau G. G-quartets direct assembly of HIV-1 nucleocapsid protein along single-stranded DNA. Nucleic Acids Res. 2003; 31:5754–5763. [PubMed: 14500839]
15. Sundquist WI, Heaphy S. Evidence for interstrand quadruplex formation in the dimerization of human immunodeficiency virus 1 genomic RNA. Proc Natl Acad Sci U S A. 1993; 90:3393–3397. [PubMed: 8475087]
16. Pereira LA, Bentley K, Peeters A, Churchill MJ, Deacon NJ. A compilation of cellular transcription factor interactions with the HIV-1 LTR promoter. Nucleic Acids Res. 2000; 28:663–668. [PubMed: 10637316]
17. Burnett JC, Miller-Jensen K, Shah PS, Arkin AP, Schaffer DV. Control of stochastic gene expression by host factors at the HIV promoter. PLoS Pathog. 2009; 5:e1000260. [PubMed: 19132086]
18. Feng S, Holland EC. HIV-1 tat trans-activation requires the loop sequence within tar. Nature. 1988; 334:165–167. [PubMed: 3386755]

19. Feinberg MB, Baltimore D, Frankel AD. The role of Tat in the human immunodeficiency virus life cycle indicates a primary effect on transcriptional elongation. Proc Natl Acad Sci U S A. 1991; 88:4045–4049. [PubMed: 2023953]
20. de Arellano ER, Alcami J, Lopez M, Soriano V, Holguin A. Drastic decrease of transcription activity due to hypermutated long terminal repeat (LTR) region in different HIV-1 subtypes and recombinants. Antiviral Res. 2010; 88:152–159. [PubMed: 20713090]
21. Michael NL, D'Arcy L, Ehrenberg PK, Redfield RR. Naturally occurring genotypes of the human immunodeficiency virus type 1 long terminal repeat display a wide range of basal and Tat-induced transcriptional activities. J Virol. 1994; 68:3163–3174. [PubMed: 7908701]
22. Jeeninga RE, Hoogenkamp M, Armand-Ugon M, de Baar M, Verhoef K, Berkhout B. Functional differences between the long terminal repeat transcriptional promoters of human immunodeficiency virus type 1 subtypes A through G. J Virol. 2000; 74:3740–3751. [PubMed: 10729149]
23. Kikin O, D'Antonio L, Bagga PS. QGRS Mapper: a web-based server for predicting G-quadruplexes in nucleotide sequences. Nucleic Acids Res. 2006; 34:W676–W682. [PubMed: 16845096]
24. Karsisiotis AI, Hessari NM, Novellino E, Spada GP, Randazzo A, Webba da Silva M. Topological characterization of nucleic acid G-quadruplexes by UV absorption and circular dichroism. Angew Chem Int Ed Engl. 2011; 50:10645–10648. [PubMed: 21928459]
25. Vorlickova M, Kejnovska I, Sagi J, Renciuk D, Bednarova K, Motlova J, Kypr J. Circular dichroism and guanine quadruplexes. Methods. 2012; 57:64–75. [PubMed: 22450044]
26. Mergny JL, Li J, Lacroix L, Amrane S, Chaires JB. Thermal difference spectra: a specific signature for nucleic acid structures. Nucleic Acids Res. 2005; 33:e138. [PubMed: 16157860]
27. Nadai M, Palu G, Palumbo M, Richter SN. Differential Targeting of Unpaired Bases within Duplex DNA by the Natural Compound Clerocidin: A Valuable Tool to Dissect DNA Secondary Structure. PLoS One. 2012; 7:e52994. [PubMed: 23285245]
28. Nadai M, Sattin G, Palu G, Palumbo M, Richter SN. Clerocidin-mediated DNA footprinting discriminates among different G-quadruplex conformations and detects tetraplex folding in a duplex environment. Biochim. Biophys Acta-Gen. Subj. 2013; 1830:4660–4668.
29. Han H, Langley DR, Rangan A, Hurley LH. Selective interactions of cationic porphyrins with G-quadruplex structures. J Am Chem Soc. 2001; 123:8902–8913. [PubMed: 11552797]
30. Qin Y, Fortin JS, Tye D, Gleason-Guzman M, Brooks TA, Hurley LH. Molecular cloning of the human platelet-derived growth factor receptor beta (PDGFR-beta) promoter and drug targeting of the G-quadruplex-forming region to repress PDGFR-beta expression. Biochemistry. 2010; 49:4208–4219. [PubMed: 20377208]
31. Palumbo SL, Ebbinghaus SW, Hurley LH. Formation of a unique end-to-end stacked pair of G-quadruplexes in the hTERT core promoter with implications for inhibition of telomerase by G-quadruplex-interactive ligands. J Am Chem Soc. 2009; 131:10878–10891. [PubMed: 19601575]
32. Yu Z, Gaerig V, Cui Y, Kang H, Gokhale V, Zhao Y, Hurley LH, Mao H. Tertiary DNA structure in the single-stranded hTERT promoter fragment unfolds and refolds by parallel pathways via cooperative or sequential events. J Am Chem Soc. 2012; 134:5157–5164. [PubMed: 22372563]
33. Mukundan VT, Phan AT. Bulges in G-Quadruplexes: Broadening the Definition of G-Quadruplex-Forming Sequences. J Am Chem Soc. 2013; 135:5017–5028.
34. Siddiqui-Jain A, Grand CL, Bearss DJ, Hurley LH. Direct evidence for a G-quadruplex in a promoter region and its targeting with a small molecule to repress c-MYC transcription. Proc Natl Acad Sci U S A. 2002; 99:11593–11598. [PubMed: 12195017]
35. Membrino A, Cogoi S, Pedersen EB, Xodo LE. G4-DNA formation in the HRAS promoter and rational design of decoy oligonucleotides for cancer therapy. PLoS One. 2011; 6:e24421. [PubMed: 21931711]
36. Basundra R, Kumar A, Amrane S, Verma A, Phan AT, Chowdhury S. A novel G-quadruplex motif modulates promoter activity of human thymidine kinase 1. Febs J. 2010; 277:4254–4264. [PubMed: 20849417]
37. Derdeyn CA, Decker JM, Sfakianos JN, Wu X, O'Brien WA, Ratner L, Kappes JC, Shaw GM, Hunter E. Sensitivity of human immunodeficiency virus type 1 to the fusion inhibitor T-20 is

modulated by coreceptor specificity defined by the V3 loop of gp120. J Virol. 2000; 74:8358–8367. [PubMed: 10954535]

38. Emert-Sedlak LA, Narute P, Shu ST, Poe JA, Shi H, Yanamala N, Alvarado JJ, Lazo JS, Yeh JI, Johnston PA, Smithgall TE. Effector kinase coupling enables high-throughput screens for direct HIV-1 Nef antagonists with antiretroviral activity. Chem Biol. 2013; 20:82–91. [PubMed: 23352142]
39. Qin Y, Hurley LH. Structures, folding patterns, and functions of intramolecular DNA G-quadruplexes found in eukaryotic promoter regions. Biochimie. 2008; 90:1149–1171. [PubMed: 18355457]
40. Cogoi S, Xodo LE. G-quadruplex formation within the promoter of the KRAS proto-oncogene and its effect on transcription. Nucleic Acids Res. 2006; 34:2536–2549. [PubMed: 16687659]
41. Qin Y, Rezler EM, Gokhale V, Sun D, Hurley LH. Characterization of the G-quadruplexes in the duplex nuclease hypersensitive element of the PDGF-A promoter and modulation of PDGF-A promoter activity by TMPyP4. Nucleic Acids Res. 2007; 35:7698–7713. [PubMed: 17984069]
42. McLuckie KI, Waller ZA, Sanders DA, Alves D, Rodriguez R, Dash J, McKenzie GJ, Venkitaraman AR, Balasubramanian S. G-quadruplex-binding benzo[a]phenoxazines down-regulate c-KIT expression in human gastric carcinoma cells. J Am Chem Soc. 2011; 133:2658–2663. [PubMed: 21294544]
43. Greenfield NJ. Using circular dichroism collected as a function of temperature to determine the thermodynamics of protein unfolding and binding interactions. Nat Protoc. 2006; 1:2527–2535. [PubMed: 17406506]
44. Doria F, Nadai M, Folini M, Scalabrin M, Germani L, Sattin G, Mella M, Palumbo M, Zaffaroni N, Fabris D, Freccero M, Richter SN. Targeting loop adenines in G-quadruplex by a selective oxirane. Chem. Eur. J. 2013; 19:78–81. [PubMed: 23212868]
45. Emert-Sedlak L, Kodama T, Lerner EC, Dai W, Foster C, Day BW, Lazo JS, Smithgall TE. Chemical library screens targeting an HIV-1 accessory factor/host cell kinase complex identify novel antiretroviral compounds. ACS Chem Biol. 2009; 4:939–947. [PubMed: 19807124]
46. Poe JA, Smithgall TE. HIV-1 Nef dimerization is required for Nef-mediated receptor downregulation and viral replication. J Mol Biol. 2009; 394:329–342. [PubMed: 19781555]

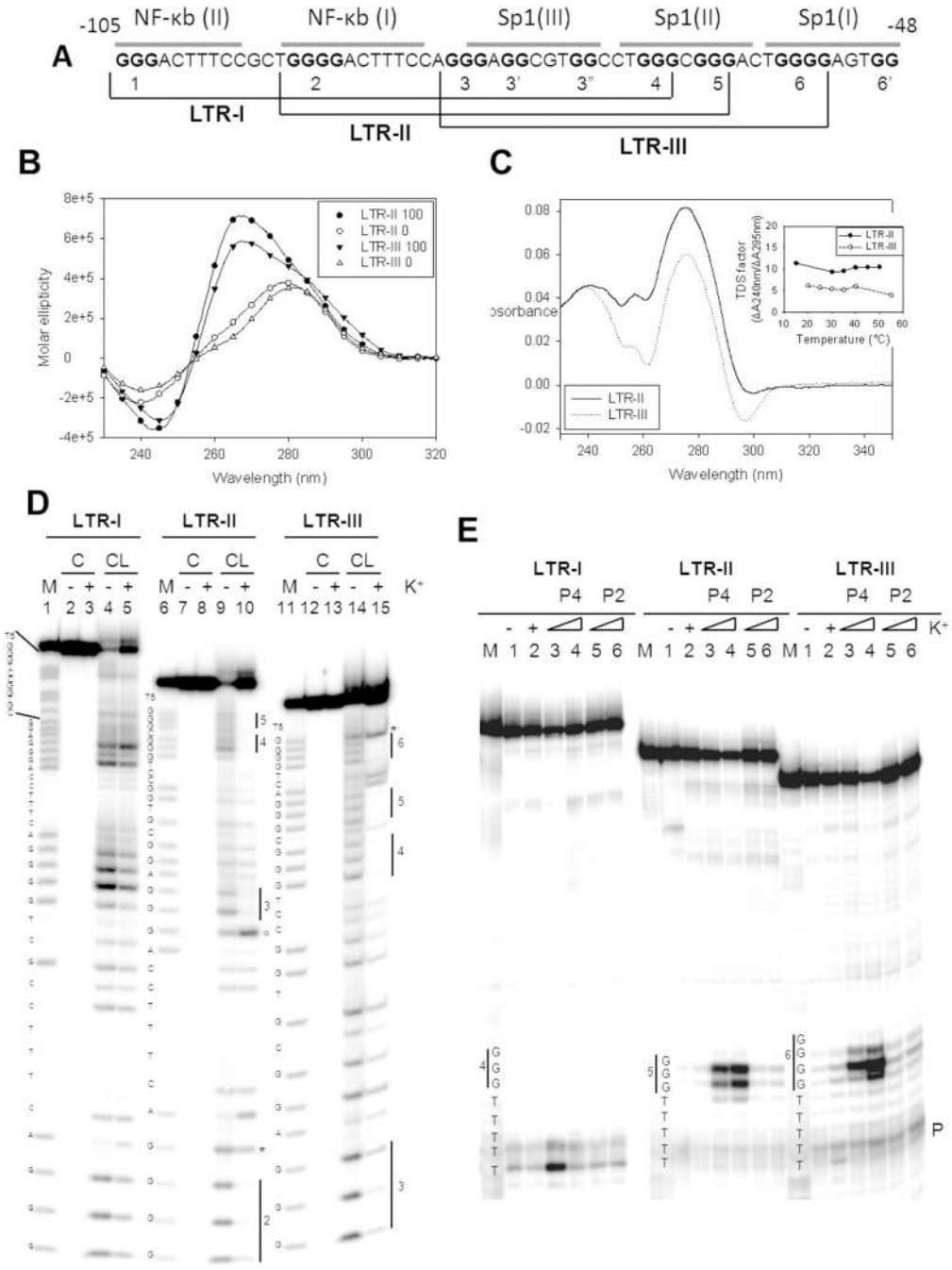

Figure 1.

Characterization of LTR-I, LTR-II and LTR-III G-quadruplexes. A) Sequence of the G-rich LTR region spanning −105/−48 nts. G bases involved in G-quadruplex are in bold. G-tracts are numbered. Brackets indicate sequences that form G-quadruplexes with 3 stacked tetrads. B) CD spectra in the absence (0) or presence (100) of K^+. C) Thermal difference spectra (TDS) $A_{95°C}/A_t$. TDS factor graph ($\Delta A_{240nm}/\Delta A_{295nm}$ of absorbance above and below the melting) is shown in the inset. D) Clerocidin-protection assay. LTR sequences renatured in the presence or absence of K^+, were treated with clerocidin followed by hot piperidine to induce cleavage at the G alkylated sites (CL lanes) or just treated with hot piperidine (C lanes). Base sequences are provided on the left of each oligonucleotide (5'-end shown at the

bottom). Protected G-tracts are indicated with vertical lines and corresponding numbers (see Fig. 1). The ¤ symbol indicate overexposed bases and the * symbol indicate non-protected bases within a protected G-tract. M are the marker lanes. E) Taq polymerase stop assay. Oligonucleotides were folded in the presence or absence of K^+. K^+-treated samples were further incubated with either TMPyP4 (P4) or the control compound TMPyP2 (P2). Oligonucleotides were used as templates in a Taq polymerase reaction at 45°C. Bases at the 3'-end and the corresponding 3'-G-tract are indicated for each sequence. P indicates the band of the labelled primer. M is a marker lane obtained with the Maxam&Gilbert sequencing protocol.

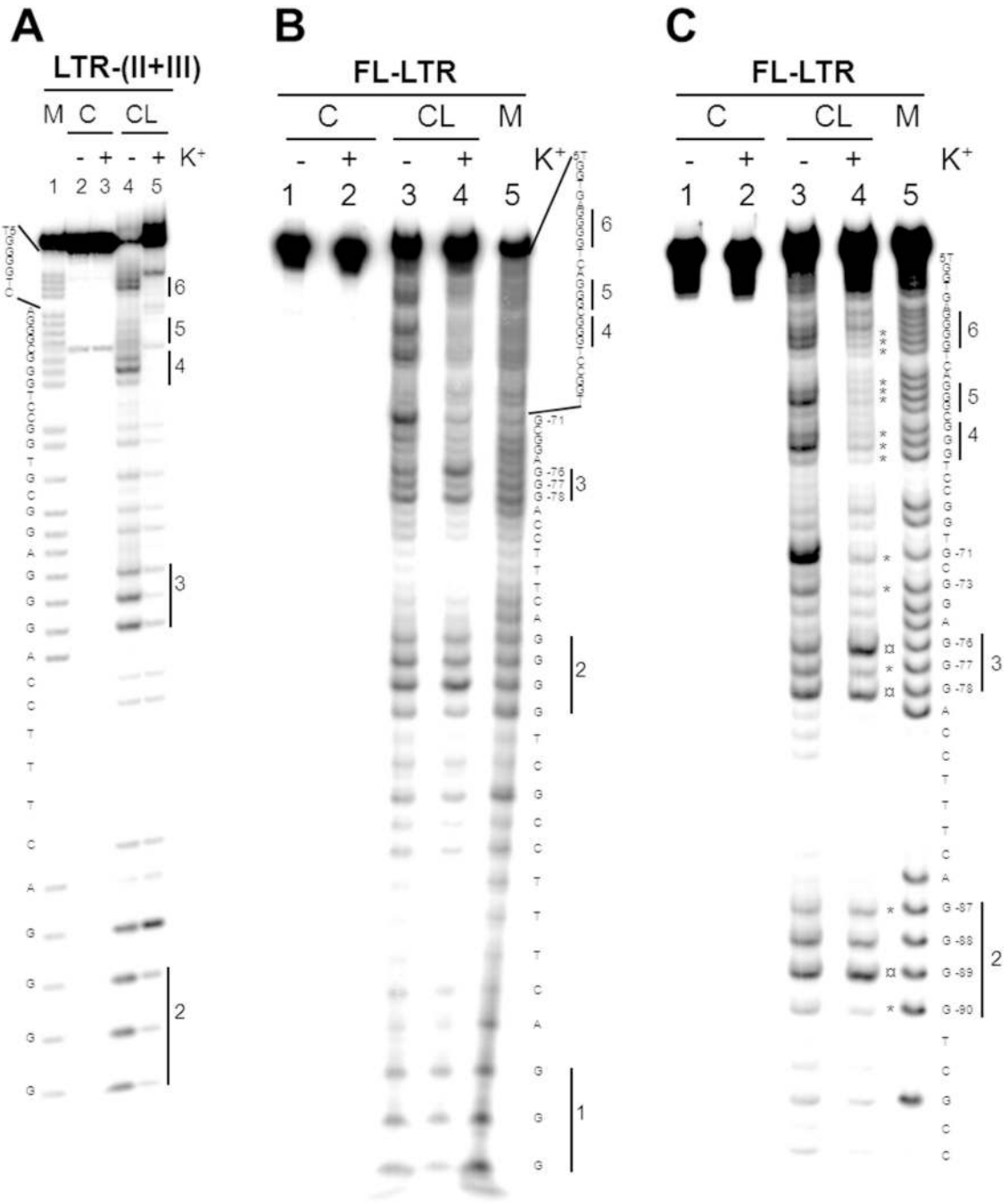

Figure 2.

Characterization of G-quadruplex structures in extended regions of the LTR G-rich sequence. A) The LTR-(II+III) oligonucleotide and B) the FL-LTR sequence were folded in the presence or absence of K^+ and treated with CL followed by hot piperidine (CL lanes) or just treated with piperidine (C lanes). Relevant G-tracts are highlighted by vertical lines and corresponding numbers. M indicates the marker lane. Base sequences are shown aside each gel image. C) Magnification of the 3'-end of the FL-LTR oligonucleotide. Samples were treated as described above but they were run for shorter time in the denaturing gel. The * and ¤ symbols indicate protected and overexposed nucleotides, respectively.

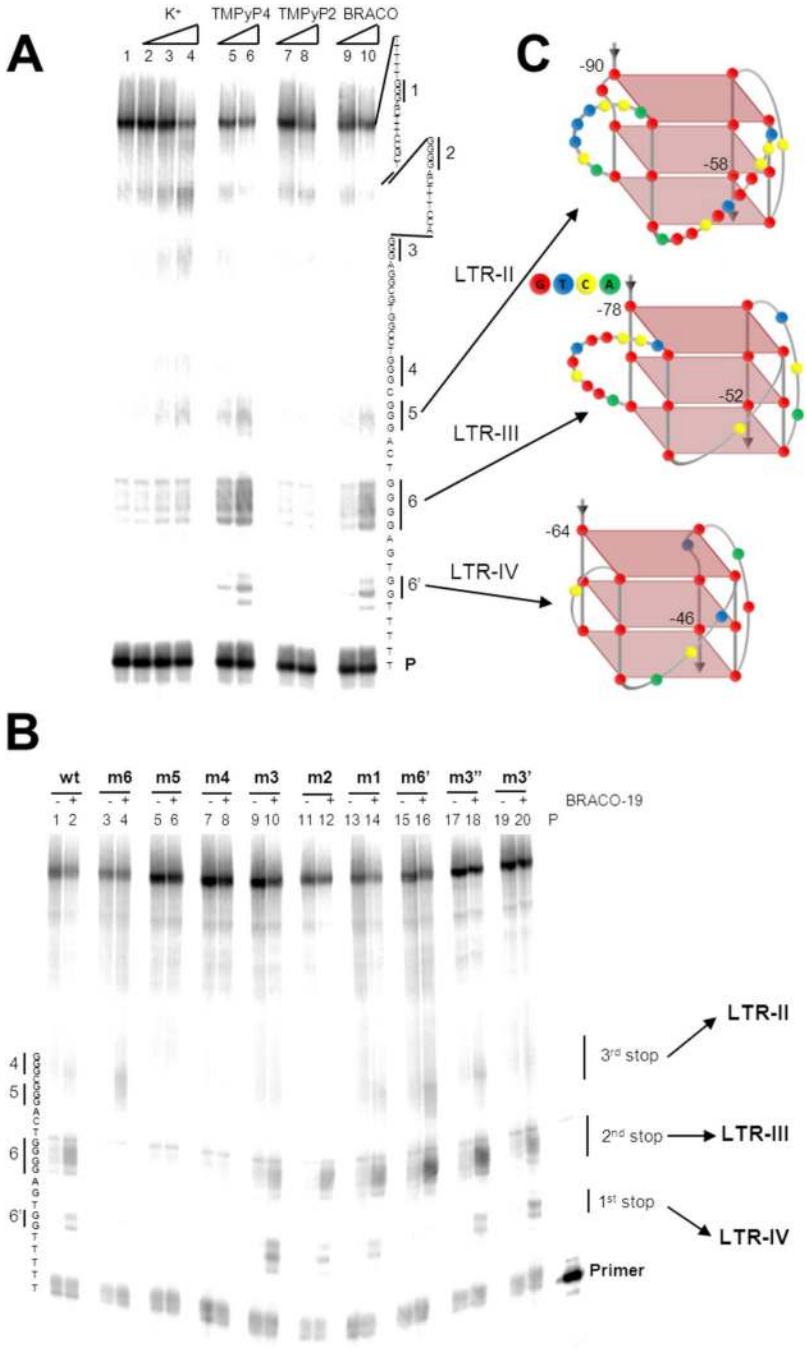

Figure 3.

G-quadruplexes forming in the FL-LTR sequence. A) Taq polymerase stop assay on the FL-LTR template in the presence of increasing concentration of K^+ (0–150 mM) (lanes 1–4) and of 100 mM K^+ and G-quadruplex ligands TMPyP4 (lanes 5–6), TMPyP2 (lanes 7–8) and BRACO-19 (lanes 9–10). The base sequence is shown on the right. Vertical lines indicate stop sites observed in the presence of K^+. Arrows point to the structures of G-quadruplexes stabilized in the presence of G-quadruplex ligands. B) Taq polymerase stop assay on the wild-type and mutants FL-LTR templates in the presence of 100 mM K^+ and 100 nM BRACO-19. C) Models of characterized LTR G-quadruplex structures. G, T, C, and

A bases are shown in red, blue, yellow and green, respectively. Numbers in the structures indicate nucleotide position within the HIV-1 integrated genome.

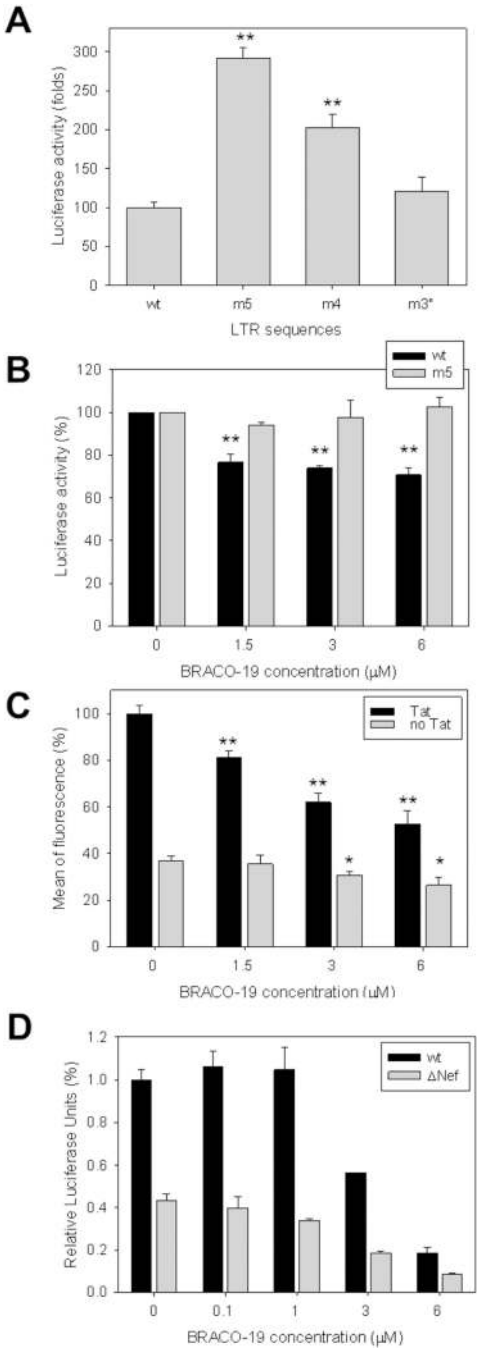

Figure 4.

Biological and antiviral effects of LTR G-quadruplexes and treatment with G-quadruplex ligands. A) Luciferase expression of the wild-type and mutant LTRs normalized to the *Renilla* luciferase expression and to the wild-type sequence in HEK 293T cells. B) Normalized luciferase expression of the WT and m5 LTRs in the presence of BRACO-19 (1.5–6.0 μM). C) GFP mean of fluorescence of cells transfected with the WT LTR-GFP plasmid and treated with increasing concentration (1.5–6.0 μM) of BRACO-19 in the absence or presence of Tat. In all data sets: $n = 3$, mean ± s.d., Student's t-test, $^{*}P < 0.05$, $^{**}P < 0.01$. D) TZM-bl cells were infected with wild-type (black bars) and ΔNef (grey bars) HIV NL4-3 in the presence of the G-4 stabilizing ligand, BRACO-19. After 48 h, levels of

gene expression were assessed as relative luciferase activity in infected cells. Results are shown relative to the wild-type control cells incubated with only the carrier solvent (DMSO) ± SEM (n = 3). Significant inhibtion ($P < 0.05$) was observed at 3 and 6 μM for both wild-type and Δ*Nef* infected cells.

Table 1

Stabilization (T_m) of LTR sequences (4 μM) in the absence and presence of 100 mM K^+ and G-quadruplex ligands (16 μM).

G-quadruplex sequence	K^+ (mM)	Drug added	T_m (°C)	ΔT_m (°C) ($Tm_{K^+[100]} - Tm_{K^+[0]}$)	ΔT_m (°C) ($Tm_{K^+[100]}$ drug $- Tm_{K^+[100]}$)
LTR-II	0	-	39.7 ± 1.2	-	-
	0	T	52.1 ± 1.8	-	12.4
	0	B	57.3 ± 1.7	-	17.6
	0	P	53.5 ± 4.0	-	13.8
	100	-	49.0 ± 0.2	9.3	-
	100	T	82.4 ± 1.5	30.3	33.4
	100	B	88.9 ± 0.6	31.6	39.9
	100	P	80.1 ± 3.3	26.6	31.1
LTR-III	0	-	38.0 ± 1.5	-	
	0	T	60.9 ± 2.5	-	22.9
	0	B	50.9 ± 1.1	-	12.9
	0	P	53.0 ± 1.2	-	15
	100	-	51.9 ± 0.2	13.9	-
	100	T	89.9 ± 0.7	29	38
	100	B	94.2 ± 2.0	43.3	42.3
	100	P	68.3 ± 1.3	15.3	16.4
LTR-(II+III)	0	-	34.4 ± 2.0	-	-
	100	-	55.8 ± 0.3	21.4	-
LTR-FL	0	-	33.8 ± 5.1	-	-
	100	-	56.6 ± 0.8	22.8	-
	100	T	61.1 ± 0.5	-	4.5
	100	B	62.2 ± 0.5	-	5.6
	100	P	65.4 ± 0.4	-	8.8
LTR-IV	0	-	26.2 ± 0.5	-	-

G-quadruplex sequence	K^+ (mM)	Drug added	T_m (°C)	ΔT_m (°C) ($Tm_{K^+[100]} - Tm_{K^+[0]}$)	ΔT_m (°C) ($Tm_{K^+[100]\ drug} - Tm_{K^+[100]}$)
	100	-	43.4 ± 0.2	17.2	-
	100	T	87.3 ± 3.4	-	43.9
	100	B	97.4 ± 3.2	-	54.0
	100	P	99.2 ± 6.5	-	55.8

T = TMPyP4, B = BRACO-19, P = PIPER